Published in final edited form as:
Cancer Res. 2007 October 1; 67(19): 9435–9442. doi:10.1158/0008-5472.CAN-07-1316.

Malignant Progression and Blockade of Angiogenesis in a Murine Transgenic Model of Neuroblastoma

Louis Chesler[1,5], **David D. Goldenberg**[2], **Isha T. Seales**[2], **Ronit Satchi-Fainaro**[7], **Matt Grimmer**[1], **Rodney Collins**[6], **Chris Struett**[2], **Kim N. Nguyen**[2], **Grace Kim**[6], **Tarik Tihan**[6], **Yun Bao**[2], **Rolf A. Brekken**[8], **Gabriele Bergers**[3,4,5], **Judah Folkman**[9], and **William A. Weiss**[1,2,3,4,5]

[1] Department of Pediatrics, University of California-San Francisco Medical School, San Francisco, California

[2] Department of Neurology, University of California-San Francisco Medical School, San Francisco, California

[3] Department of Neurological Surgery, University of California-San Francisco Medical School, San Francisco, California

[4] Brain Tumor Research Center, University of California-San Francisco Medical School, San Francisco, California

[5] Comprehensive Cancer Center, University of California-San Francisco Medical School, San Francisco, California

[6] Department of Pathology, University of California-San Francisco Medical School, San Francisco, California

[7] Department of Physiology and Pharmacology, Sackler School of Medicine, Tel Aviv University, Tel Aviv, Israel

[8] Departments of Surgery and Pharmacology, Hamon Center for Therapeutic Oncology Research, University of Texas Southwestern Medical Center, Dallas, Texas

[9] Departments of Surgery and Cellular Biology, Harvard Medical School and Children's Hospital, Boston, Massachusetts

Abstract

Targeted expression of *MYCN* to the neural crest [under control of the rat tyrosine hydroxylase (TH) promoter] causes neuroblastoma in transgenic mice (TH-*MYCN*) and is a well-established model for this disease. Because high levels of *MYCN* are associated with enhanced tumor angiogenesis and poor clinical outcome in neuroblastoma, we serially characterized malignant progression, angiogenesis, and sensitivity to angiogenic blockade in tumors from these animals. Tumor cells were proliferative, secreted high levels of the angiogenic ligand vascular endothelial growth factor (VEGF), and recruited a complex vasculature expressing the angiogenic markers VEGF-R2, α-SMA, and matrix metalloproteinases MMP-2 and MMP-9, all of which are also expressed in human disease. Treatment of established murine tumors with the angiogenesis inhibitor TNP-470 caused near-complete ablation, with reduced proliferation, enhanced apoptosis,

Requests for reprints: William A. Weiss, Department of Neurology, University of California-San Francisco, 533 Parnassus Avenue, Room U441O, San Francisco, CA 94143. Phone: 415-502-1694; Fax: 415-476-0133; weiss@cgl.ucsf.edu.
L. Chesler and D.D. Goldenberg contributed equally to this work.

Note: Supplementary data for this article are available at Cancer Research Online (http://cancerres.aacrjournals.org/).

and vasculature disruption. Because TNP-470 has been associated with neurotoxicity, we tested the recently described water-soluble HPMA copolymer–TNP-470 conjugate (caplostatin), which showed comparable efficacy and was well tolerated without weight loss or neurotoxicity as measured by rotarod testing. This study highlights the importance of angiogenesis inhibition in a spontaneous murine tumor with native tumor–microenvironment interactions, validates the use of mice transgenic for TH-*MYCN* as a model for therapy in this common pediatric tumor, and supports further clinical development of caplostatin as an antiangiogenic therapy in childhood neuroblastoma.

Introduction

Neuroblastoma is the most common extracranial solid tumor of childhood (1,2). Approximately one third of tumors show amplification of *MYCN*, a genetic abnormality closely associated with poor outcome (1). High-risk tumors amplified for *MYCN* typically show a paucity of stromal elements, compared with tumors diploid for *MYCN*, which are stroma rich and less aggressive (1,3). Although these observations suggest that cells in the microenvironment influence the behavior of transformed neuroblasts, the factors contributing to this process in neuroblastoma remain poorly understood.

The acquisition of tumor-derived vasculature is a critical example of tumor-microenvironment interactions in cancer (4). Potential mechanisms through which neuroblast-specific expression of *MYCN* induces angiogenesis in the surrounding microenvironment include activation of vascular endothelial growth factor (VEGF) and the proangiogenic matrix metalloproteinase-2 (MMP-2) and repression of the angiogenesis inhibitors thrombospondin, activin-A, and angiopoietin, all of which act on endothelial cells (5–12). These observations suggest that neuroblasts in this embryonal tumor signal to the microenvironment to promote angiogenesis, that Mycn protein itself is critical to angiogenesis in the subset of high-risk tumors that show amplification of *MYCN*, and that relevant models of tumor-microenvironment interactions are needed to test targeted therapy in general and antiangiogenic therapies in particular in this disease.

We previously generated a model for high-risk, *MYCN*-amplified neuroblastoma by directing expression of *MYCN* to the peripheral neural crest of transgenic mice under control of the rat tyrosine hydroxylase (TH) promoter (13). Mice transgenic for TH-*MYCN* in the 129/SvJ background develop tumors in peripheral neural crest-derived structures and show the typical histopathologic features of human neuroblastoma. Genome-wide screens of tumor tissue revealed localized gains of mouse chromosome 11 (orthologous to gains on human chromosome 17q commonly observed in human tumors), clustered loss of chromosomes 5, 9, and 16 (syntenic to an analogous clustered loss of chromosomes 3p, 4p, and 11q in human tumors), and amplification of the TH-*MYCN* transgene (14–16). Significantly, these mice replicate the microenvironmental architecture characteristic of human *MYCN*-amplified tumors. Because the effect of *MYCN* on neuroblasts is highly context specific, interactions between tumor and host-derived stromal components (e.g., infiltrating Schwann cells and host-secreted metalloproteinases) have a major effect on tumor biology and responses to therapy (17). These critical interactions between the tumor and its microenvironment reinforce the importance of species-matched interactions between host and stromal elements.

To develop these mice as a platform for targeted therapy and to exploit species-matched interactions between tumor and microenvironment in this native model, we characterized malignant progression and neovascularization in murine tumors hemizygous for the *MYCN* transgene. Animals with tumors were divided into three groups: early (group I), intermediate

(group II), and advanced (group III). Within this framework, we assessed indices of proliferation, apoptosis, and vascularity and correlated these with the expression of markers known in human tumors to be associated with malignant progression in tumor cells and with angiogenesis in the microenvironment. We next evaluated sensitivity to antiangiogenic therapy. Remarkably, and in contrast with published data using human tumors xenografted into immunocompromised mice (18–21), the antiangiogenic fumagillin analogue TNP-470 led to near-complete regression of advanced tumors. The HPMA copolymer–conjugated form of TNP-470 (caplostatin) was equally effective and is an attractive agent for clinical use due to its favorable pharmacokinetics, nontoxic profile, and water solubility. These studies establish the importance of interactions between tumor and microenvironment in a species-matched immunocompetent mouse model for this common peripheral nervous system tumor and suggest that caplostatin should be further tested clinically in the treatment of childhood neuroblastoma.

Materials and Methods

Tissue preparation

Mice were anesthetized and either lectin perfused or sacrificed without perfusion. Tumor tissues were embedded and flash frozen immediately after excision. Lectin-perfused animals received a retroorbital injection of 1 μL/g of rhodamine-conjugated RCAI lectin (Vector Laboratories). Animals were then perfused with 4% paraformaldehyde (Fisher) at 15 mL/min, followed by further perfusion with PBS at the same rate. Both flash frozen and lectin-perfused tissues were sectioned at 10-μm thickness, mounted and stored at −80°C. All experiments were approved by the University of California-San Francisco Institutional Animal Care and Use Committee.

Immunocytochemical staining

Frozen sections were fixed in 4% paraformaldehyde. Tissues were blocked for 1 h in 0.5% Tween (Fisher), 2% bovine serum albumin (Sigma Chemical Co.), and 5% normal horse or goat serum (Jackson ImmunoResearch, Inc.) and then incubated with primary antisera and dilutions: monoclonal rat anti-mouse CD31 antibody (BD PharMingen, Inc.), 1:500; polyclonal rabbit antisera to all isoforms of VEGF (Neomarker, Inc.), 1:300; polyclonal rabbit antisera to VEGF-R2 (22), 10 μg/mL; polyclonal rabbit anti-human MMP-2 (Chemicon, Inc.), 1:50; monoclonal mouse anti–α-SMA clone 1A4 (Sigma), 1:1,000; polyclonal rabbit antisera to Ki67 (Novocastra, Inc.), 1:500. Secondary antibodies included Cy-2–conjugated donkey anti-rat, Cy-3–conjugated donkey anti-rabbit, or Cy-3 donkey anti-mouse (all from Jackson ImmunoResearch; 1:200).

Quantification of proliferation and apoptosis

Immunofluorescent images were examined using MetaMorph 6.1 (Molecular Devices Corp.). In representative slides from tumors of each group, immunofluorescence for TUNEL, bis-benzimide, or Ki67 was separately quantified in five fields. Results were averaged for tumors of each group. The Student's *t* test was used to evaluate statistical significance. Apoptotic cells were identified using the DEADEND Fluorometric TUNEL System (Promega, Inc.). Tissues were sectioned at 4 μm and stained with Gill's hematoxylin III (American Master Tech Scientific, Inc.) and 1% alcoholic eosin (Sigma). H&E-stained tissues were viewed with an Axioskop 2 FS+, and images were captured with an AxioCam HR (Carl Zeiss MicroImaging, Inc.). Immunofluorescence was viewed and photographed with a Confocal Laser Scanning Microscope 510 NLO (Zeiss).

Reverse transcription-PCR

Tumor tissues were flash frozen and stored at −80°C. Total RNA was extracted using Trizol reagent (Invitrogen, Inc.), and 6 μg of total RNA were reverse transcribed using Superscript II RNaseH H^- (Invitrogen). Expression of MMP-9 and L-19 (loading control) was assessed after 30 cycles using the primers indicated (Supplementary Fig. S1).

Treatment of mice with TNP-470 and caplostatin

Animals hemizygous for the *MYCN* transgene with palpable, intermediate group tumors (~60 days of life) were treated three times per week with i.p. injections of TNP-470 (100 mg/kg in 100 μL DMSO) or DMSO alone for 2 weeks (eight animals per group). At sacrifice, tumors were excised, measured, weighed, snapped-frozen for immunoblotting, fixed in 10% buffered formalin for paraffin embedding or fresh-frozen for immunohistochemistry of frozen sections. Mice were weighed daily to monitor for drug toxicity. Weight loss was limited to 15% by institutional protocol. Treatment was terminated at 2 weeks when three animals in the treated group had weight loss above the cutoff (Supplementary Fig. S2). Caplostatin experiments were done similarly at an i.p. TNP-470 equivalent dose of 50 mg/kg dissolved in saline. This dose (50% of the dose used for unconjugated TNP-470 experiments) is similar to dosing of caplostatin used in other animal models.

Evaluation of neurotoxicity

Neurotoxicity was monitored using a rotarod assay, which uses a rotating treadmill (Medical Associates, Inc.), to assess coordination and balance. Before and after 1 and 2 weeks of therapy with caplostatin, mice were first placed on the rotarod for 30 s to permit acclimation. Mice were then replaced on the rotarod at a standard acceleration rate of 3 rotations/min/s. Time on the treadmill (hang time) was recorded for each animal.

Statistical methods

In vitro data are expressed as means ± SDs, and *in vivo* data as means ± SE. Statistical significance testing used the Student's *t* test. For detected differences, the Wilcoxon rank-sum test was used to assess pairwise differences between treatment groups, with $P < 0.05$ considered to be statistically significant.

Results

Malignant progression in mice transgenic for TH-*MYCN*

We dissected a cohort of 60 animals hemizygous for the *MYCN* transgene in strain 129X1/SvJ at ages ranging from 44 to 80 days (Fig. 1*A*). Four or more animals were analyzed by full necropsy at each time point. In this strain, tumor onset was reproducible and confined to a narrow age window (Fig. 1*A*). Penetrance for tumors was 65% by 95 days (Fig. 1*B*). Tumors arising in the mice were classified according to size and degree of regional spread analogous in these two characteristics to the staging of primary human neuroblastoma (23).

Localized tumors (group I) arose between 45 and 55 days of life (Fig. 1*C* and *D*), were small and spherical (approximately the size of a kidney), showed no regional organ invasion, and were not easily palpated (analogous to stage I tumors in humans). Intermediate tumors (group II) arose between 55 and 65 days of life and were 1.5 to 2 kidney diameters, adherent to major blood vessels and organs, and easily palpable (analogous to stage II tumors in humans; Fig. 1*E* and *F*). Organ margins were negative for tumor by histologic analysis (data not shown). Advanced tumors (group III) arose after 65 days, were grossly visible in the absence of palpation, and, on necropsy, crossed the midline, reminiscent of stage III tumors

in humans in size and degree of regional involvement (Fig. 1*G* and *H*). Tumor histology was similar in all groups (Fig. 1*D, F*, and *H*), revealing a predominance of small, round, blue tumor cells (neuroblasts) in a stroma-poor background, with an abundance of tumor-associated blood vessels of varying caliber. Tumor-associated vessels in group III lesions, in general, were more dilated, with a larger cross-sectional vessel diameter. There was no difference in vascular leakage between group I and group III lesions visible on unperfused H&E-stained tumor sections, except in areas of localized tumor necrosis, which were more readily apparent in group III lesions (Fig. 1*H*, inset) and were rare in other groups. Local spread to lymph nodes was observed in all groups (Fig. 1*I*). Whereas gross metastases were rare, microscopic metastases to the liver and kidney were seen in four of four animals with group III tumors (Fig. 1*J*).

Proliferation, detected by nuclear localization of Ki67 antigen, was high in all groups (Fig. 2*A–C*). TUNEL staining of apoptotic nuclei (Fig. 2*D–F*) increased significantly in group III compared with group I ($P < 0.001$), consistent with the structural findings of areas of increased cell death and focal apoptosis on H&E staining (Fig. 1*D, F, and H*). There was no statistical difference in TUNEL positivity between group I and II. The increased apoptosis in advanced tumors likely reflects an inability of these lesions to maintain adequate tissue perfusion and oxygen tension, a characteristic common to large solid tumors (24). Levels of MYCN mRNA were assessed by reverse transcription-PCR (RT-PCR) and did not differ among groups (data not shown).

Murine neuroblastoma is highly vascularized

To evaluate vascularity, mice with palpable tumors were analyzed by perfusion fixation with rhodamine-conjugated lectin, followed by immunofluorescent analysis using antisera to platelet-endothelial cell adhesion molecule (CD31). Tumors displayed a rich vasculature (Fig. 2*G–J*). Rare small vessels stained for CD31 in the absence of rhodamine immunofluorescence (Fig. 2*H–J*, arrows) indicating nonfunctioning vessels. Although vasculature was plentiful in all tumors (Fig. 3*A–C*), vessels seemed dilated and more irregular within advanced lesions (Fig. 3*A–C*). Periendothelial cells were visualized using antisera to smooth muscle actin (α-SMA) and colocalized to the CD31-stained vasculature in all groups (Fig. 3*D–F*). There were no quantifiable differences in vascular pericyte coverage between group I and group III tumors. Tumor cells in all groups showed strong cytoplasmic immunoreactivity for VEGF ligand (Fig. 3*G–I*). To assess VEGF-R2 expression in endothelial cells, tumor tissues were stained with antisera against CD31 and VEGF-R2. Colocalization of CD31 and VEGF-R2 immunoreactivity was illustrated in all groups (Fig. 3*J–L*). Antisera to MMP-2 showed cytoplasmic staining that associated closely with CD31 positive endothelial cells lining the blood vessels (Fig. 3*M–O*). The immunoreactivity of MMP-9 could not be adequately assessed using commercial antisera. By RT-PCR, expression of MMP-9 mRNA increased in group III tumors, compared with tumors in groups I and II (Supplementary Fig. S1).

Efficacy of angiogenesis inhibitors in murine neuroblastoma

The robust vascularity common to both murine and high-risk *MYCN*-amplified human neuroblastoma led us to test whether angiogenesis inhibitors could show efficacy. We treated established murine tumors using TNP-470, a methionine aminopeptidase-2 inhibitor with defined activity against xenografted human neuroblastoma (19–21,25–28). Groups of eight animals with intermediate tumors were treated with TNP-470 (100 mg/kg i.p. thrice weekly) or placebo for 2 weeks, when euthanasia was required due to significant weight loss in treated animals (Supplementary Fig. S2).

Tumors showed a striking response to therapy compared with placebo-treated controls (Fig. 4*A* and compare *B* and *C*). Marked changes were observed in the histologic appearance and immunohistochemical features of tumors treated with TNP-470 (Fig. 4*D–K*). The characteristic lobular appearance of tumor neuroblasts with surrounding intact blood vessels was replaced by grossly visible hemorrhagic areas with increased apoptosis and necrosis (Fig. 4, compare *D* and *H*). On immunohistochemical analysis of paraffin-embedded sections, treated tumors showed reduced staining for the proliferative marker Ki67, except in well-perfused areas surrounding large blood vessels (compare Fig. 4*E* and *I*), supporting a role for vascular integrity in maintaining proliferation of these tumors. The degree of apoptosis, assessed by staining of cleaved caspase-3, was greatly increased by TNP-470 treatment (compare Fig. 4*F* and *J*), again with sparing of neuroblasts in perivascular locations (arrows). Disruption of the perilobular distribution of small blood vessels was readily apparent (compared by CD31 staining in Fig. 4*G* and *K*), consistent with angiogenic blockade effecting small vessels to a greater degree than large vessels. Taken together, these findings imply that TNP-470 targets vascular integrity in established neuroblastoma tumors with a secondary effect on parenchymal neuroblasts, resulting in eradication of tumor parenchyma through apoptosis and necrosis.

Significant weight loss requiring euthanasia (>15%) was observed in treated animals (average weight, 21 ± 2 g in treated animals versus 28 ± 3 g average in controls, $P < 0.01$). Because neurotoxicity and associated weight loss preclude the use of TNP-470 clinically, we next tested HPMA copolymerized TNP-470 (caplostatin), a water-soluble form of TNP-470 that does not cross the blood-brain barrier, and that is better tolerated in preclinical models (29,30). Caplostatin was also highly effective as a single agent against established tumors (Fig. 5*A* and compare *B* and *C*). No statistically significant weight loss was observed in caplostatin-treated animals (Supplementary Fig. S2). Furthermore, caplostatin-treated animals displayed similar retention time on the rotarod assay compared with control mice (Supplementary Fig. S3), indicative of normal coordination and balance, and abrogation of the neurotoxicity associated with free TNP-470 (29,30).

Discussion

Pediatric embryonal tumor formation fails to conform to established paradigms for malignant progression (31). Whereas aggressive tumors of the brain or colon may arise through the sequential acquisition of malignant characteristics (32,33), low-risk neuroblastoma tumors diploid for *MYCN* generally do not progress to high-risk disease *MYCN*-amplified disease (1). In fact, the clinical presentation of neuroblastoma is consistent with a nonlinear model, through which neuroblast progenitors follow one of several distinct pathways to transformation, leading to tumors of low, intermediate, and high-risk, respectively. Amplification of *MYCN* is associated with advanced disease and is the best-characterized genetic marker of high-risk neuroblastoma (1). The association of *MYCN* amplification with aggressive disease suggests that transformed neuroblasts fail to respond to differentiating signals, a process normally associated with down-regulation of Mycn (34).

Within the confines of a murine tumor that models *MYCN*-amplified neuroblastoma in children, we developed a classification that incorporates tumor size and local invasiveness. Tumor cell proliferation did not change between groups and was therefore not incorporated. Both apoptosis and metastases increased as a function of tumor size, as observed in high-risk tumors in children (35). The increased levels of apoptosis in large murine tumors are also observed in other advanced human neoplasms (36–38). Collectively, these observations suggest that murine neuroblastoma driven by a TH-*MYCN* transgene closely models a subset of childhood neuroblastoma amplified for *MYCN*, leading to similarly aggressive and poorly differentiated malignancies.

Whereas xenograft models for neuroblastoma have been valuable for testing cytotoxic chemotherapy, the species-mismatched microenvironment has potential limitations for evaluation of targeted antiangiogenic agents. Transgenic mouse models have proved useful for stepwise mechanistic analyses of interactions between tumor and vascular compartments, for studying the effects of inhibiting angiogenesis, and for assessing the effect of such interventions on tumor cells (4,39,40). In contrast to flank xenograft models, tumors in mice transgenic for TH-*MYCN* arise in a species-matched immunocompetent host, in comparable locations to those in children with neuroblastoma (suprarenal, abdominal or thoracic paraspinal ganglia), show genetic heterogeneity typical of human disease (13–16,41), and coopt a species-matched vasculature. These variables, as well as the clinical importance of this tumor in children (the most common extracranial solid tumor of childhood), provide a compelling rationale to develop TH-*MYCN* transgenic mice as a platform for developmental therapeutics in neuroblastoma.

Given the prominence of interactions between *MYCN*-driven neuroblasts and the neighboring microenvironment, targeted agents that disrupt these interactions hold great potential for therapy. Childhood *MYCN*-amplified neuroblastoma is typically a vascular tumor, with much of this neovascularization mediated by interactions between *MYCN*-amplified neuroblasts and the local microenvironment. Perfusion-fixation of murine tumors with rhodamine and CD31 also documents a comparably complex vasculature mirroring that observed in human disease. Expression of VEGF has been reported in primary neuroblasts from human neuroblastoma, whereas expressions of VEGF-R1, VEGF-R2, MMP2, MMP9, and α-SMA are expressed in endothelial and periendothelial cells within the tumor microenvironment (5,6,11,42–46). All of these proteins were also expressed in appropriate tumor and stromal elements from mice transgenic for TH-*MYCN*.

The sensitivity of these tumors to TNP-470 and the HPMA copolymer caplostatin is marked and is more profound than previous reports of the activity of this and other antiangiogenic agents using human xenograft models for neuroblastoma (19–21,25–28,47–49). That an antiangiogenic agent affects the progression of established aggressive neuroblastomas bodes well for comparable agents as components of therapy for disease in humans. TNP-470 itself has shown some toxicity in preclinical and clinical trials. Caplostatin abrogates this toxicity (29,30) and therefore should be an attractive agent for a phase I clinical study in neuroblastoma.

Supplementary Material

Refer to Web version on PubMed Central for supplementary material.

Acknowledgments

Grant support: NIH grants R01CA102321, P30HD28825, K08NS053530-01A3, Campini Family Foundation, Thrasher Research Fund, and Samuel Waxman Cancer Research Foundation.

We thank Nadezhda Milshteyn for genotyping, dissections, and for preservation of tumor samples, Jane Gordon for help with confocal microscope, Steven Song for RT-PCR primers, Patrick McQuillen for assistance with Metamorph Software, and Chris Hackett and Anders Persson for critical review of the manuscript.

References

1. Brodeur, GM.; Maris, JM. Neuroblastoma. In: Pizzo, PA.; Poplack, DG., editors. Principles and Practice of Pediatric Oncology. 4. Philadelphia: J. B. Lippincott Company; 2002. p. 895-938.
2. Maris JM, Hogarty MD, Bagakell R, Cohn SL. Neuroblastoma. Lancet 2007;369:2106–20. [PubMed: 17586306]

3. Shimada H, Chatten J, Newton W Jr, et al. Histopathologic prognostic factors in neuroblastic tumors: definition of subtypes of ganglioneuroblastoma and an age-linked classification of neuroblastomas. J Natl Cancer Inst 1984;732:405–16. [PubMed: 6589432]
4. Hanahan D, Folkman J. Patterns and emerging mechanisms of the angiogenic switch during tumorigenesis. Cell 1996;86:353–64. [PubMed: 8756718]
5. Sugiura Y, Shimada H, Seeger RC, Laug WE, DeClerck YA. Matrix metalloproteinases-2 and -9 are expressed in human neuroblastoma: contribution of stromal cells to their production and correlation with metastasis. Cancer Res 1998;5810:2209–16. [PubMed: 9605768]
6. Ara T, Fukuzawa M, Kusafuka T, et al. Immunohistochemical expression of MMP-2, MMP-9, and TIMP-2 in neuroblastoma: association with tumor progression and clinical outcome. J Pediatr Surg 1998;338:1272–8. [PubMed: 9722003]
7. Watnick RS, Cheng YN, Rangarajan A, Ince TA, Weinberg RA. Ras modulates Myc activity to repress thrombospondin-1 expression and increase tumor angiogenesis. Cancer Cell 2003;33:219–31. [PubMed: 12676581]
8. Ribatti D, Raffaghello L, Pastorino F, et al. *In vivo* angiogenic activity of neuroblastoma correlates with MYCN oncogene overexpression. Int J Cancer 2002;1024:351–4. [PubMed: 12402304]
9. Schramm A, von Schuetz V, Christiansen H, et al. High activin A-expression in human neuroblastoma: suppression of malignant potential and correlation with favourable clinical outcome. Oncogene 2005;244:680–7. [PubMed: 15580313]
10. Holash J, Maisonpierre PC, Compton D, et al. Vessel cooption, regression, and growth in tumors mediated by angiopoietins and VEGF. Science 1999;2845422:1994–8. [PubMed: 10373119]
11. Chantrain CF, Shimada H, Jodele S, et al. Stromal matrix metalloproteinase-9 regulates the vascular architecture in neuroblastoma by promoting pericyte recruitment. Cancer Res 2004;645:1675–86. [PubMed: 14996727]
12. Ribatti D, Marimpietri D, Pastorino F, et al. Angiogenesis in neuroblastoma. Annals of the New York Academy of Sciences 2004;1028:133–42. [PubMed: 15650239]
13. Weiss WA, Aldape K, Mohapatra G, Feuerstein BG, Bishop JM. Targeted expression of MYCN causes neuroblastoma in transgenic mice. EMBO J 1997;1611:2985–95. [PubMed: 9214616]
14. Weiss WA, Godfrey T, Francisco C, Bishop JM. Genome-wide screen for allelic imbalance in a mouse model for neuroblastoma. Cancer Res 2000;609:2483–7. [PubMed: 10811128]
15. Hackett CS, Hodgson JG, Law ME, et al. Genome-wide array CGH analysis of murine neuroblastoma reveals distinct genomic aberrations which parallel those in human tumors. Cancer Res 2003;6317:5266–73. [PubMed: 14500357]
16. Norris MD, Burkhart CA, Marshall GM, Weiss WA, Haber M. Expression of N-myc and MRP genes and their relationship to N-myc gene dosage and tumor formation in a murine neuroblastoma model. Med Pediatr Oncol 2000;356:585–9. [PubMed: 11107123]
17. Ambros IM, Zellner A, Roald B, et al. Role of ploidy, chromosome 1p, and Schwann cells in the maturation of neuroblastoma. N Engl J Med 1996;33423:1505–11. [PubMed: 8618605]
18. Wassberg E, Christofferson R. Angiostatic treatment of neuroblastoma. Eur J Cancer 1997;3312:2020–3. [PubMed: 9516846]
19. Katzenstein HM, Rademaker AW, Senger C, et al. Effectiveness of the angiogenesis inhibitor TNP-470 in reducing the growth of human neuroblastoma in nude mice inversely correlates with tumor burden. Clin Cancer Res 1999;512:4273–8. [PubMed: 10632370]
20. Katzenstein HM, Salwen HR, Nguyen NN, Meitar D, Cohn SL. Antiangiogenic therapy inhibits human neuroblastoma growth. Med Pediatr Oncol 2001;361:190–3. [PubMed: 11464880]
21. Shusterman S, Grupp SA, Barr R, Carpentieri D, Zhao H, Maris JM. The angiogenesis inhibitor tnp-470 effectively inhibits human neuroblastoma xenograft growth, especially in the setting of subclinical disease. Clin Cancer Res 2001;74:977–84. [PubMed: 11309349]
22. Feng D, Nagy JA, Brekken RA, et al. Ultrastructural localization of the vascular permeability factor/vascular endothelial growth factor (VPF/VEGF) receptor-2 (FLK-1, KDR) in normal mouse kidney and in the hyper-permeable vessels induced by VPF/VEGF-expressing tumors and adenoviral vectors. J Histochem Cytochem 2000;484:545–56. [PubMed: 10727296]

23. Brodeur GM, Pritchard J, Berthold F, et al. Revisions of the international criteria for neuroblastoma diagnosis, staging, and response to treatment. J Clin Oncol 1993;118:1466–77. [PubMed: 8336186]
24. Folkman J, Greenspan HP. Influence of geometry on control of cell growth. Biochimica et biophysica acta 1975;4173–4:211–36.
25. Morowitz MJ, Barr R, Wang Q, et al. Methionine aminopeptidase 2 inhibition is an effective treatment strategy for neuroblastoma in preclinical models. Clin Cancer Res 2005;117:2680–5. [PubMed: 15814649]
26. Shusterman S, Grupp SA, Maris JM. Inhibition of tumor growth in a human neuroblastoma xenograft model with TNP-470. Med Pediatr Oncol 2000;356:673–6. [PubMed: 11107144]
27. Wassberg E, Pahlman S, Westlin JE, Christofferson R. The angiogenesis inhibitor TNP-470 reduces the growth rate of human neuroblastoma in nude rats. Pediatr Res 1997;413:327–33. [PubMed: 9078530]
28. Nagabuchi E, VanderKolk WE, Une Y, Ziegler MM. TNP-470 antiangiogenic therapy for advanced murine neuroblastoma. J Pediatr Surg 1997;322:287–93. [PubMed: 9044139]
29. Satchi-Fainaro R, Puder M, Davies JW, et al. Targeting angiogenesis with a conjugate of HPMA copolymer and TNP-470. Nat Med 2004;103:255–61. [PubMed: 14981512]
30. Satchi-Fainaro R, Mamluk R, Wang L, et al. Inhibition of vessel permeability by TNP-470 and its polymer conjugate, caplostatin. Cancer Cell 2005;73:251–61. [PubMed: 15766663]
31. Grimmer MR, Weiss WA. Childhood tumors of the nervous system as disorders of normal development. Current opinion in pediatrics 2006;186:634–8. [PubMed: 17099362]
32. Kinzler KW, Vogelstein B. Lessons from hereditary colorectal cancer. Cell 1996;87:159–70. [PubMed: 8861899]
33. Persson, A.; Fan, Q.; Phillips, JJ.; Weiss, WA. Glioma. In: Gilman, S., editor. Neurobiology of Disease. New York: Elsevier Academic Press; 2007. p. 433-44.
34. Wakamatsu Y, Watanabe Y, Nakamura H, Kondoh H. Regulation of the neural crest cell fate by N-myc: promotion of ventral migration and neuronal differentiation. Development Cambridge England 1997;12410:1953–62.
35. Joshi VV, Chatten J, Sather HN, Shimada H. Evaluation of the Shimada classification in advanced neuroblastoma with a special reference to the mitosiskaryorrhexis index: a report from the Childrens Cancer Study Group. Mod Pathol 1991;42:139–47. [PubMed: 2047378]
36. Takeda A, Perry G, Abraham NG, et al. Over-expression of heme oxygenase in neuronal cells, the possible interaction with Tau. J Biol Chem 2000;2758:5395–9. [PubMed: 10681514]
37. Vakkala M, Lahteenmaki K, Raunio H, Paakko P, Soini Y. Apoptosis during breast carcinoma progression. Clin Cancer Res 1999;52:319–24. [PubMed: 10037180]
38. Vakkala M, Paakko P, Soini Y. Expression of caspases 3, 6 and 8 is increased in parallel with apoptosis and histologic aggressiveness of the breast lesion. Br J Cancer 1999;814:592–9. [PubMed: 10574243]
39. Bergers G, Song S, Meyer-Morse N, Bergsland E, Hanahan D. Benefits of targeting both pericytes and endothelial cells in the tumor vasculature with kinase inhibitors. J Clin Invest 2003;1119:1287–95. [PubMed: 12727920]
40. Bergers G, Javaherian K, Lo KM, Folkman J, Hanahan D. Effects of angiogenesis inhibitors on multistage carcinogenesis in mice. Science 1999;2845415:808–12. [PubMed: 10221914]
41. Hansford LM, Thomas WD, Keating JM, et al. Mechanisms of embryonal tumor initiation: distinct roles for MycN expression and MYCN amplification. Proc Natl Acad Sci U S A 2004;10134:12664–9. [PubMed: 15314226]
42. Beierle EA, Dai W, Langham MR Jr, Copeland EM III, Chen MK. VEGF receptors are differentially expressed by neuroblastoma cells in culture. J Pediatr Surg 2003;383:514–21. [PubMed: 12632379]
43. Meister B, Grunebach F, Bautz F, et al. Expression of vascular endothelial growth factor (VEGF) and its receptors in human neuroblastoma. Eur J Cancer 1999;353:445–9. [PubMed: 10448297]
44. Langer I, Vertongen P, Perret J, Fontaine J, Atassi G, Robberecht P. Expression of vascular endothelial growth factor (VEGF) and VEGF receptors in human neuroblastomas. Med Pediatr Oncol 2000;346:386–93. [PubMed: 10842244]

45. Ribatti D, Surico G, Vacca A, et al. Angiogenesis extent and expression of matrix metalloproteinase-2 and -9 correlate with progression in human neuroblastoma. Life Sci 2001;6810:1161–8. [PubMed: 11228100]

46. Rossler J, Breit S, Havers W, Schweigerer L. Vascular endothelial growth factor expression in human neuroblastoma: up-regulation by hypoxia. Int J Cancer 1999;811:113–7. [PubMed: 10077161]

47. Ribatti D, Ponzoni M. Antiangiogenic strategies in neuroblastoma. Cancer Treat Rev 2005;311:27–34. [PubMed: 15707702]

48. Ribatti D, Raffaghello L, Marimpietri D, et al. Fenretinide as an anti-angiogenic agent in neuroblastoma. Cancer Lett 2003;1971–2:181–4.

49. Kuroiwa M, Ikeda H, Hongo T, et al. Effects of recombinant human endostatin on a human neuroblastoma xenograft. Int J Mol Med 2001;84:391–6. [PubMed: 11562777]

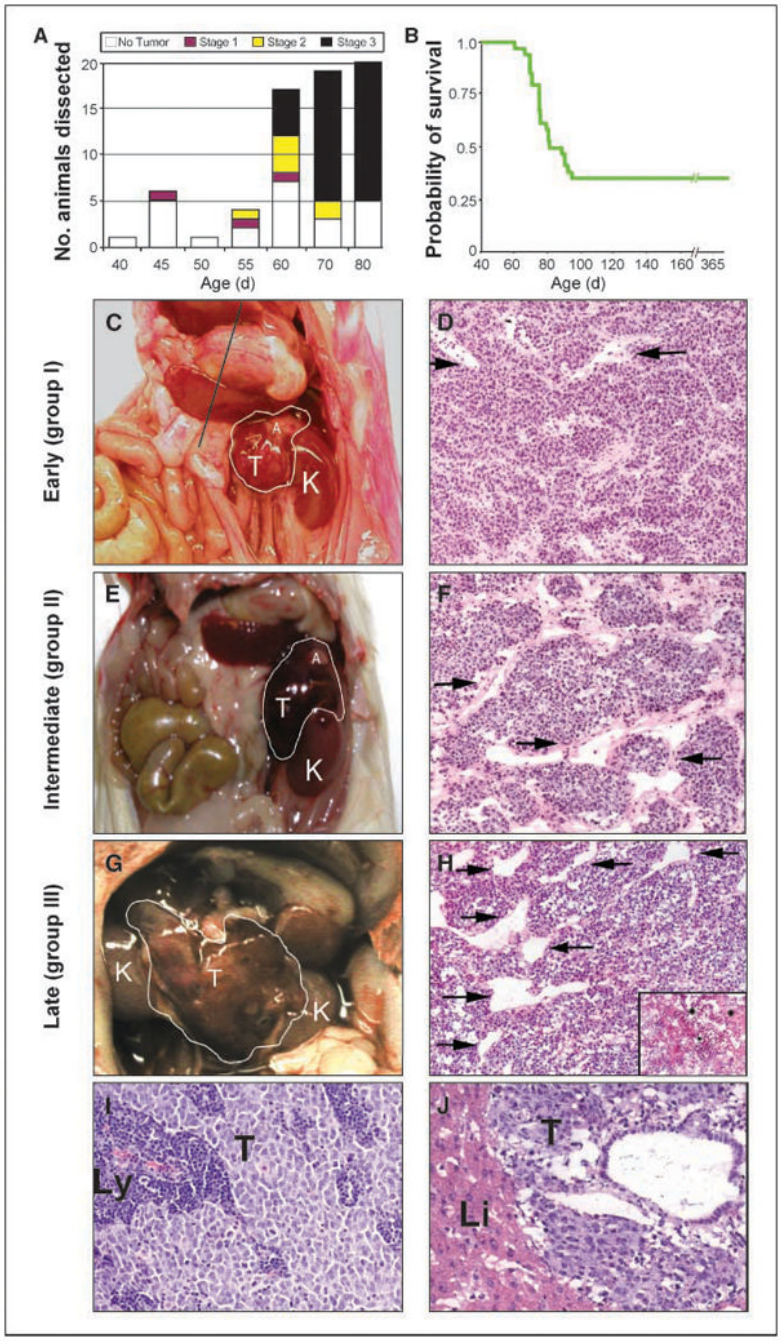

Figure 1.

Malignant progression of neuroblastoma in hemizygous mice transgenic for TH-*MYCN*. *A*, bar graph of animals dissected at specific time points illustrating the incidence of localized, intermediate, and advanced tumors. *B*, Kaplan Meier analysis shows that 65% of mice transgenic for TH-*MYCN* died of tumor by 95 d. *C*, *E*, *G*, gross appearance and grouping of murine tumors at representative ages. *D*, *F*, *H*, H&E staining illustrates similar histopathology for tumors at all groups. Vessel caliber was increased in intermediate and advanced tumors compared with localized tumors (*arrows*). Regionally spread tumors showed increased necrosis compared with localized tumors (*inset in H*). *I*, *J*, H&E staining showing localized spread to lymph nodes in a group I tumor (*I*) and distant metastasis to

liver in a group III tumor (*J*). K, kidney; T, tumor; A, adrenal gland; Li, liver; Ly, lymph node.

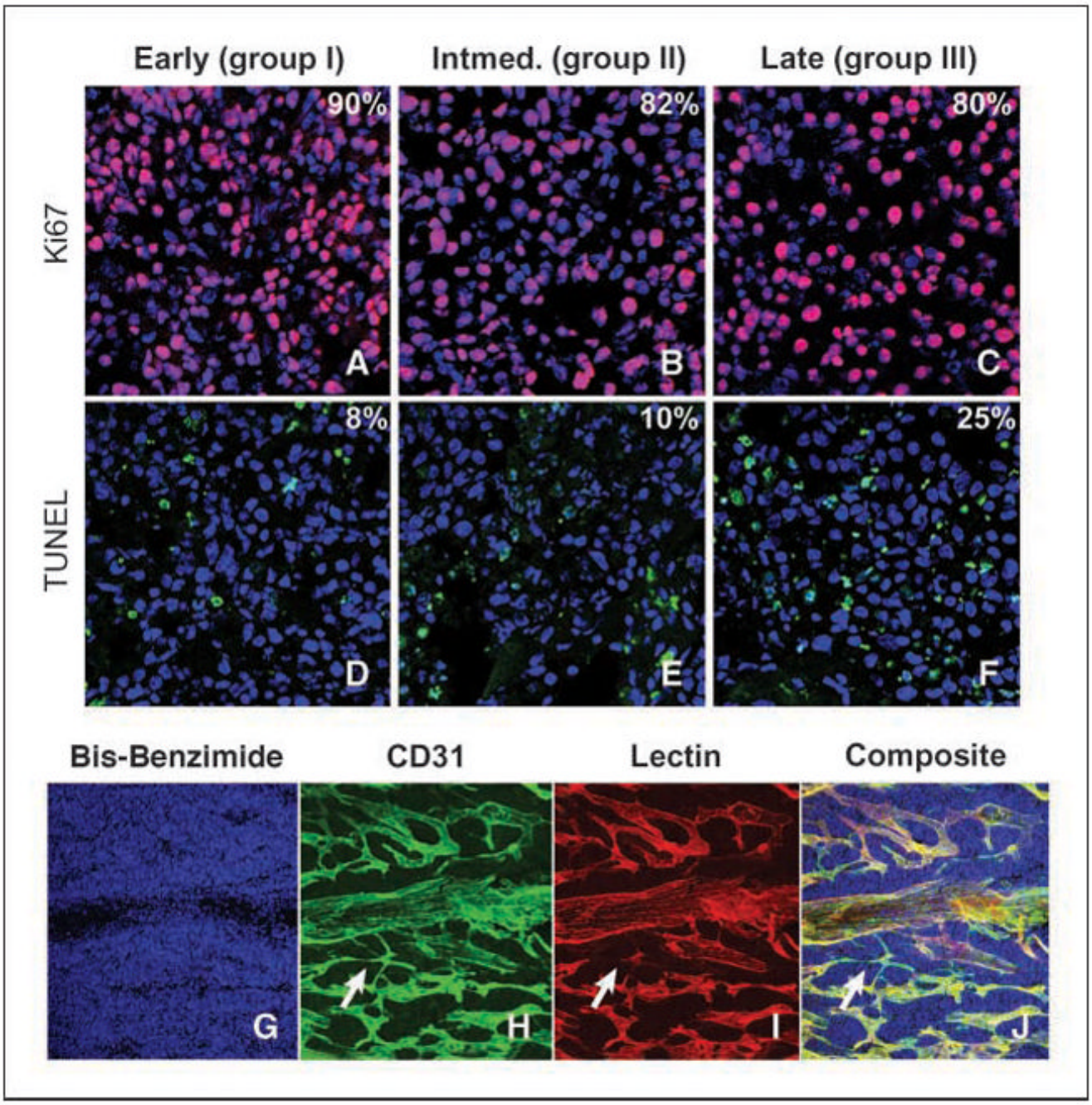

Figure 2.

Apoptosis and proliferation as a function of tumor progression. *A–F*, Ki67-positive tumor cells (*A–C; pink*) and TUNEL-positive tumor cells (*D–F; green*). *Blue*, bisbenzimide nuclear counterstain. Percentages represent positive staining for either Ki67 or TUNEL tumor cells. *G–J*, complex vasculature in murine neuroblastoma tumors; bis-benzimide nuclear counterstain (*G*), CD31 immunoreactivity (*H*), rhodamine-conjugated lectin (*I*), composite (*J*). *Arrows*, vessels positive for CD31 but negative for rhodamine-conjugated lectin. Apoptosis and proliferation were examined by confocal microscopy at 63× magnification, and vascular staining was examined at 20× magnification.

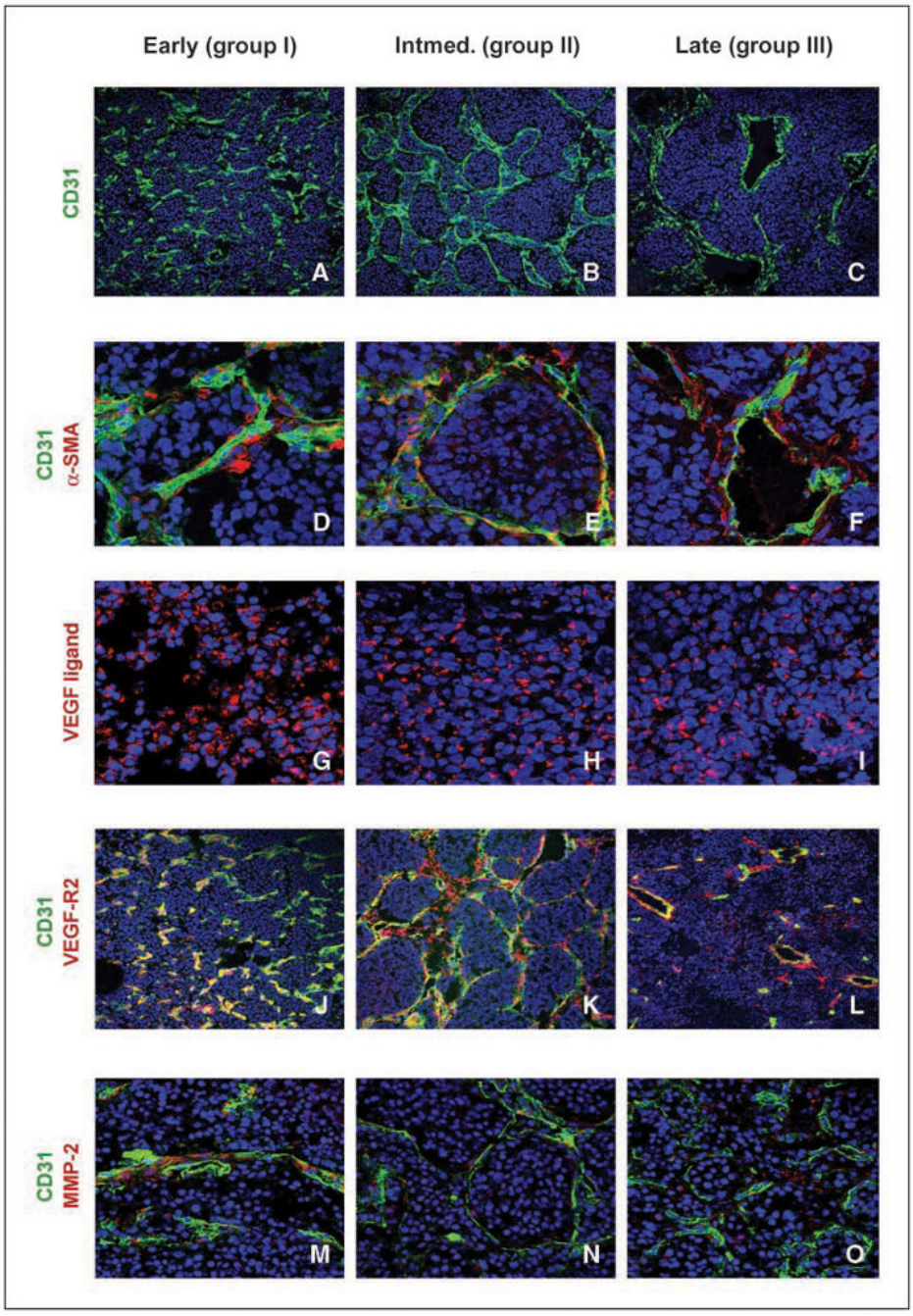

Figure 3.

Angiogenic factors contributing to murine neuroblastomas. *A–C*, CD31-positive endothelial cells (*green*) and bis-benzimide nuclear counterstain (*blue*). *D–F*, association of pericytes with endothelial cells is similar in all tumor groups. Bis-benzimide nuclear counterstain (*blue*), endothelial cells stained for α-CD31 (*green*), and α-SMA stained for pericyte positivity (*red*). *G-I*, VEGF ligand is localized in the cytoplasm and is abundant in all groups. Bis-benzimide nuclear counterstain (*blue*) and VEGF ligand (*red*). *J–L*, VEGF-R2 localizes with endothelial cells lining the blood vessels. Bis-benzimide nuclear counterstain (*blue*), endothelial cells stained for α-CD31 (*green*), and VEGF-R2 immunoreactive cells (*red*). *Yellow* represents a colocalization of endothelial cells with cells expressing VEGF-R2.

M–O, MMP-2 immunoreactivity adjacent to endothelial cells. Bis-benzimide nuclear counterstain (*blue*), CD31 endothelial cell marker (*green*), and MMP-2 immunoreactive cells (*red*). Slides examined by confocal microscope at either 20× (CD31 and VEGF-R2), 40× (VEGF ligand and MMP-2) or 63× (α-SMA) objective.

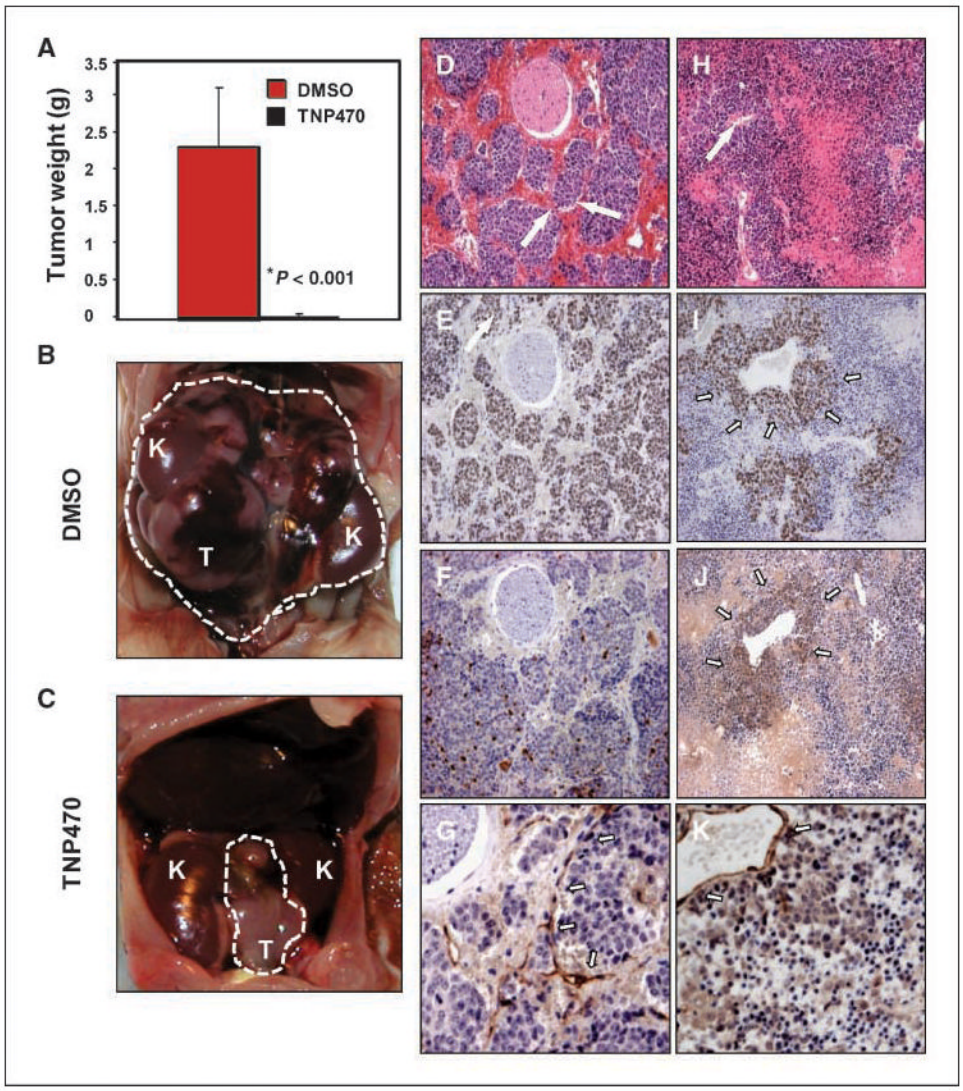

Figure 4.

Treatment of established murine neuroblastoma tumors with TNP-470. Animals with intermediate tumors were treated with either DMSO or TNP-470 (100 mg/kg i.p. thrice weekly) for 2 wks (eight per group). *A*, tumor weight was significantly reduced in the TNP-470–treated group compared with DMSO-treated controls ($P < 0.001$). *B*, DMSO-treated tumors progressed to group III. Dashed white line defines extent of tumor; *K*, kidney. *C*, TNP-470–treated tumors were grossly smaller (*arrows*). *D–K*, histologic and immunohistochemical appearance of DMSO (*D–G*) and TNP-470–treated (*H–K*) tumors. DMSO-treated tumor shows lobular neuroblasts with surrounding intact microvasculature (*D*, *arrows*). In response to treatment with TNP-470, this architecture was effaced by areas of hemorrhagic necrosis and apoptosis (*H*). *Arrow in H*, residual large caliber blood vessel. Proliferation, assessed by staining of Ki67 (*E*), was significantly reduced in response to TNP-470 treatment (*I*) and was limited to perivascular areas (*arrows in I*). Apoptosis, assessed by staining of cleaved caspase-3 (*F*), was increased in response to TNP-470 therapy (*J*). Staining pattern of the vascular marker CD31 was altered by therapy *(K)*. Arrows in *G* show linear staining pattern associated with tumor microvessels that are lost in

K, although staining of residual large vessels is maintained. *A*, *columns*, mean; *bars*, SE (*n* = 8 mice per group).

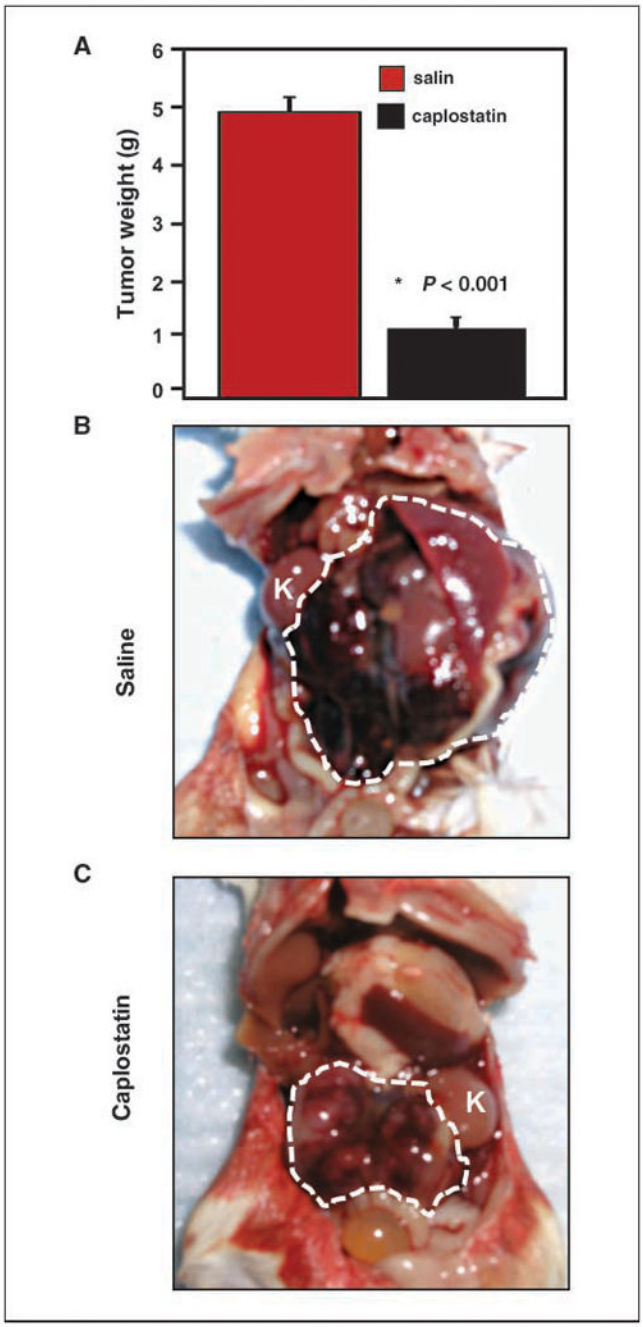

Figure 5.

Treatment of established murine neuroblastoma tumors with caplostatin (HPMA-copolymerized TNP-470). Treatment as in Fig. 4, with either saline or caplostatin (50 mg/kg TNP-470 equivalent dose, i.p. thrice weekly for 2 wks at 50% of the TNP-470 equivalent dose used in Fig. 4). *A*, tumor weight was significantly reduced ($P < 0.001$). *B*, saline-treated tumors progressed rapidly. White dashed line defines extent of tumor; *K*, kidney. *C*, caplostatin-treated tumors were grossly smaller (white dashed line defines extent of tumor). *A*, *columns*, mean; *bars*, SE ($n = 8$ mice per group).